Quasinormal mode expansion of optical far-field quantities

Felix Binkowski [●],[1] Fridtjof Betz,[1] Rémi Colom,[1] Martin Hammerschmidt [●],[2] Lin Zschiedrich [●],[2] and Sven Burger [●][1,2]

[1]*Zuse Institute Berlin, Takustraße 7, 14195 Berlin, Germany*
[2]*JCMwave GmbH, Bolivarallee 22, 14050 Berlin, Germany*

Quasinormal mode (QNM) expansion is a popular tool to analyze light-matter interaction in nanoresonators. However, expanding far-field quantities such as the energy flux is an open problem because QNMs diverge with an increasing distance to the resonant systems. We introduce a theory to compute modal expansions of far-field quantities rigorously. The presented approach is based on the complex eigenfrequencies of QNMs. The divergence problem is circumvented by using contour integration with an analytical continuation of the far-field quantity into the complex frequency plane. We demonstrate the approach by computing the angular resolved modal energy flux in the far field of a nanophotonic device.

I. INTRODUCTION

Modern nanotechnology allows for exploring new regimes in tailoring light-matter interaction [1]. Applications comprise the design of nanoantennas for quantum information technology [2], tuning photochemistry applications with nanoresonators [3], using plasmonic nanoparticles for biosensing [4], and miniaturization of optical components using dielectric metasurfaces [5]. Most approaches are based on resonance phenomena. Optical resonances are characterized by their wavelength-dependent localized and radiated field energies. They may appear as, e.g., plasmonic resonances in metals [6] or resonances in dielectric materials, such as Mie resonances [7] or bound states in the continuum [8]. The theoretical description of the resonances is essential for understanding the physical properties of the systems and for designing and optimizing related devices. A popular approach is the modeling with QNMs, which are the eigensolutions of resonant systems [9,10]. In typical nanophotonic setups, outgoing radiation conditions have to be fulfilled yielding complex eigenfrequencies and an exponential decay of the QNMs in time. This means that the QNMs diverge exponentially with an increasing distance to the resonators [9–12]. Due to the conceptual difficulties of exponential growth, this behavior has been termed "exponential catastrophe" [12]. Nevertheless, QNM-based expansion approaches, where electromagnetic fields are expanded into weighted sums of QNMs, have been derived to describe light-matter interaction in various applications [13–18]. These approaches are based on the expansion of electromagnetic fields inside and in the close vicinity of the resonators. In this way, modal near-field quantities, such as the modal Purcell enhancement [19–21], can be computed. For time-dependent problems, methods have been proposed to overcome the divergence problem [22–24].

In many applications, time-averaged far-field quantities are of special interest [1,2,5]. However, the divergence of QNMs is a key issue for modal expansion of such quantities [9,10]. From a physics perspective, for time-harmonic sources, the excited electromagnetic near- and far-field distributions are clearly nondiverging. This has motivated a discussion about the general applicability of QNMs [25]. Alternative approaches based on model approximations which yield eigenmodes with real-valued frequencies in the far-field regions have been proposed [25–27]. Further methods use the Dyson equation approach [28,29] or near-field to far-field transformations [30] of the QNMs resulting in approximations of the computed far-field quantities [18,31]. Also, the intensively discussed question of how to normalize QNMs is related to their exponential divergence [9,10,32–35].

In this work, we present a general approach for modal analysis which allows for expansions of physical observables in the far-field region. The approach is based on the complex eigenfrequencies of the resonant systems; however, the diverging behavior of the corresponding QNMs is circumvented by using contour integration of the relevant far-field quantities. Therefore, the presented approach paves the way for avoiding an exponential catastrophe while retaining the rigorous model. No approximation regarding the modeling of the naturally complex-valued frequencies of a resonant system is required. The method is validated by comparing the modal expansion to a direct solution of the corresponding scattering problem. The approach is applied to compute the modal expansion of the angular resolved energy flux density radiated to the far field by a localized source in a resonant nanostructure.

II. MODAL EXPANSION OF FAR-FIELD QUANTITIES

The QNMs of a resonant system are diverging outgoing waves. Figure 1(a) illustrates the electric field corresponding to a QNM in a one-dimensional resonator defined by layers with different refractive indices. In nano-optics, in the steady-state regime, electric fields $\mathbf{E}(\omega_0) \in \mathbb{C}^3$ are solutions to the time-harmonic Maxwell's equations in second-order form,

$$\nabla \times \mu(\omega_0)^{-1} \nabla \times \mathbf{E}(\omega_0) - \omega_0^2 \epsilon(\omega_0) \mathbf{E}(\omega_0) = i\omega_0 \mathbf{J}, \quad (1)$$

where $\omega_0 \in \mathbb{R}$ is the angular frequency and $\mathbf{J} \in \mathbb{C}^3$ is the source field. For a simpler notation, we omit the spatial
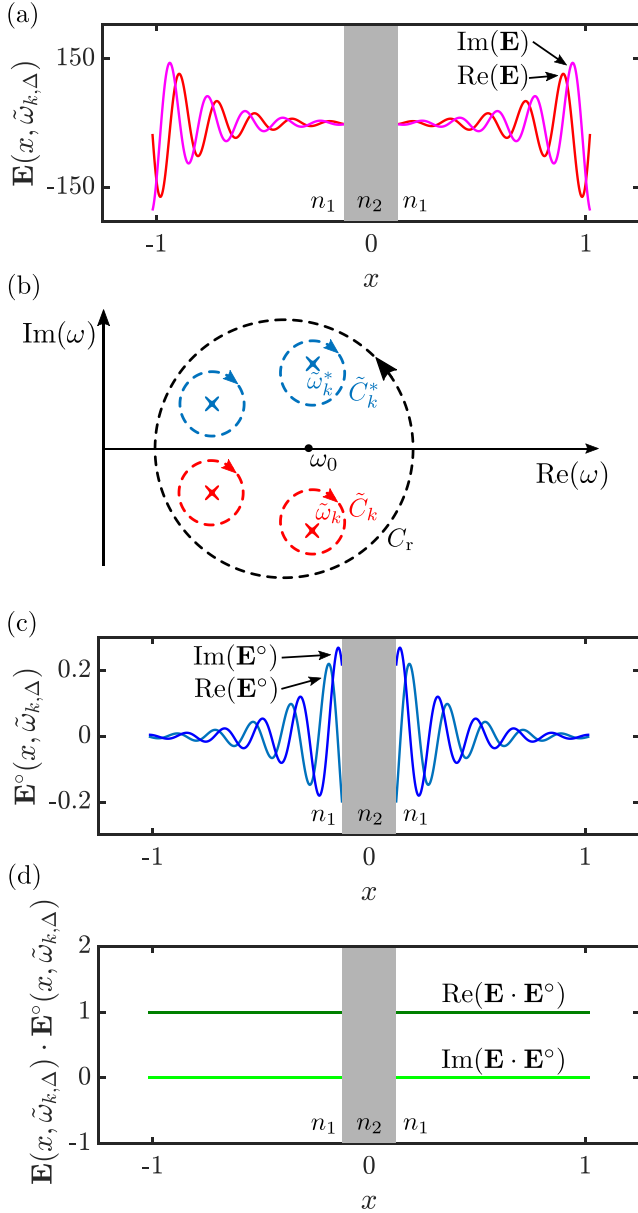
FIG. 1. One-dimensional resonator defined by layers with different refractive indices, where $n_2 > n_1$. Electric field solutions, $\mathbf{E}(x, \omega)$ and $\mathbf{E}^\circ(x, \omega)$, are obtained by solving the Helmholtz equation with a source term corresponding to incoming plane waves with unit amplitude. Only scattered fields (a.u.) outside the resonator are shown. (a) Diverging field $\mathbf{E}(x, \tilde{\omega}_{k,\Delta}) = A\, e^{i(n_1\tilde{\omega}_{k,\Delta}/c)|x|}$, where $\tilde{\omega}_k$ is a resonance pole of $\mathbf{E}(x, \omega)$ and $\tilde{\omega}_{k,\Delta} = \tilde{\omega}_k + \Delta\tilde{\omega}_k$ is a frequency close to $\tilde{\omega}_k$. (b) Illustration of resonance poles and integration contours corresponding to the RPE for the energy flux density given by Eq. (2). The analytical continuation of the energy flux density has resonance poles with negative and with positive imaginary parts. (c) Nondiverging field $\mathbf{E}^\circ(x, \tilde{\omega}_{k,\Delta}) = B\, e^{-i(n_1\tilde{\omega}_{k,\Delta}/c)|x|}$. (d) Constant product $\mathbf{E}(x, \tilde{\omega}_{k,\Delta}) \cdot \mathbf{E}^\circ(x, \tilde{\omega}_{k,\Delta})$, which relates to the energy flux density.

dependence of the quantities and write, e.g., $\mathbf{E}(\omega_0)$ instead of $\mathbf{E}(\mathbf{r}, \omega_0)$, where $\mathbf{r} \in \mathbb{R}^3$ is the position. The permittivity tensor and the permeability tensor are defined by $\epsilon(\omega_0)$ and $\mu(\omega_0)$, respectively. For optical frequencies, $\mu(\omega_0)$ is typically equal

to the vacuum permeability μ_0. QNMs are solutions to Eq. (1) equipped with outgoing radiation conditions and without a source, i.e., $\mathbf{J} = 0$. The eigenfrequencies $\tilde{\omega}_k \in \mathbb{C}$ have negative imaginary parts and are given by the complex resonance poles of the analytical continuation $\mathbf{E}(\omega)$ of the electric field $\mathbf{E}(\omega_0)$ into the complex plane $\omega \in \mathbb{C}$.

We use the Riesz projection expansion (RPE) [17,36] for modal expansion of the energy flux density in the far field, which can be expressed as a quadratic form with a sesquilinear map. The energy flux density [37] is defined by

$$s(\mathbf{E}(\omega_0), \mathbf{E}^*(\omega_0)) = \frac{1}{2}\mathrm{Re}\left(\mathbf{E}^*(\omega_0) \times \frac{1}{i\omega_0\mu_0}\nabla \times \mathbf{E}(\omega_0)\right) \cdot \mathbf{n},$$

where $\mathbf{E}^*(\omega_0)$ is the complex conjugate of the electric field and $\mathbf{n}$ is the normal on the corresponding far-field sphere. The RPE is based on contour integration in the complex frequency plane. Since the complex conjugation of the electric field makes $s(\mathbf{E}(\omega_0), \mathbf{E}^*(\omega_0))$ nonholomorphic, the evaluation of this function for complex frequencies is problematic. This challenge can be addressed by exploiting the relation $\mathbf{E}^*(\omega_0) = \mathbf{E}(-\omega_0)$ for $\omega_0 \in \mathbb{R}$. The field $\mathbf{E}(-\omega_0)$ is a solution to Eq. (1) as well. For the harmonic time dependency $e^{-i\omega_0 t}$ with a negative frequency, the radiation conditions are sign inverted. The field $\mathbf{E}(-\omega_0)$ has an analytical continuation into the complex plane $\omega \in \mathbb{C}$, which we denote by $\mathbf{E}^\circ(\omega)$. This yields the required analytical continuation of $s(\mathbf{E}(\omega_0), \mathbf{E}^*(\omega_0))$, which is given by $s(\mathbf{E}(\omega), \mathbf{E}^\circ(\omega))$. Note that $\mathbf{E}^\circ(\omega)$ introduces resonance poles in the upper complex half-plane, which are usually not considered in the literature. These poles are an essential part of the presented approach. To expand $s(\mathbf{E}(\omega_0), \mathbf{E}^*(\omega_0)) = s(\mathbf{E}(\omega_0), \mathbf{E}^\circ(\omega_0))$ into modal contributions, Cauchy's integral formula,

$$s(\mathbf{E}(\omega_0), \mathbf{E}^\circ(\omega_0)) = \frac{1}{2\pi i}\oint_{C_0} \frac{s(\mathbf{E}(\omega), \mathbf{E}^\circ(\omega))}{\omega - \omega_0}d\omega,$$

is then exploited. The contour C_0 is a closed integration path around ω_0 so that $s(\mathbf{E}(\omega), \mathbf{E}^\circ(\omega))$ is holomorphic inside of C_0. Deforming the integration path and applying Cauchy's residue theorem yield

$$s(\mathbf{E}(\omega_0), \mathbf{E}^\circ(\omega_0)) = -\sum_{k=1}^{K} \frac{1}{2\pi i}\oint_{\tilde{C}_k} \frac{s(\mathbf{E}(\omega), \mathbf{E}^\circ(\omega))}{\omega - \omega_0}d\omega$$
$$-\sum_{k=1}^{K} \frac{1}{2\pi i}\oint_{\tilde{C}_k^*} \frac{s(\mathbf{E}(\omega), \mathbf{E}^\circ(\omega))}{\omega - \omega_0}d\omega$$
$$+\frac{1}{2\pi i}\oint_{C_r} \frac{s(\mathbf{E}(\omega), \mathbf{E}^\circ(\omega))}{\omega - \omega_0}d\omega, \quad (2)$$

where $\tilde{C}_1, \ldots, \tilde{C}_K$ are contours around the resonance poles of $\mathbf{E}(\omega)$, given by $\tilde{\omega}_1, \ldots, \tilde{\omega}_K$, and $\tilde{C}_1^*, \ldots, \tilde{C}_K^*$ are contours around the resonance poles of $\mathbf{E}^\circ(\omega)$, given by $\tilde{\omega}_1^*, \ldots, \tilde{\omega}_K^*$. The outer contour C_r includes ω_0, the resonance poles $\tilde{\omega}_1, \ldots, \tilde{\omega}_K$ and $\tilde{\omega}_1^*, \ldots, \tilde{\omega}_K^*$, and no further poles, as sketched in Fig. 1(b). The Riesz projections

$$\tilde{s}_k(\mathbf{E}(\omega_0), \mathbf{E}^\circ(\omega_0)) = -\frac{1}{2\pi i}\oint_{\tilde{C}_k} \frac{s(\mathbf{E}(\omega), \mathbf{E}^\circ(\omega))}{\omega - \omega_0}d\omega$$
$$-\frac{1}{2\pi i}\oint_{\tilde{C}_k^*} \frac{s(\mathbf{E}(\omega), \mathbf{E}^\circ(\omega))}{\omega - \omega_0}d\omega$$

TABLE I. Eigenfrequencies of the resonator shown in Fig. 2(a). The eigenfrequencies $\tilde{\omega}_k$ are contained in the circular contour C_r, which is centered at 1.41×10^{15} s^{-1} and has a radius of 6.8×10^{13} s^{-1}.

k	Re($\tilde{\omega}_k$) (10^{15} s^{-1})	Im($\tilde{\omega}_k$) (10^{13} s^{-1})
1	1.441	-0.109
2	1.428	-0.182
3	1.399	-0.232
4	1.372	-0.568
5	1.370	-1.025
6	1.398	-2.475
7	1.406	-0.470
8	1.422	-0.875
9	1.435	-1.942

are modal contributions for the energy flux density. The Riesz projections $\tilde{s}_k(\mathbf{E}(\omega_0), \mathbf{E}^\circ(\omega_0))$ are associated with the eigenfrequencies $\tilde{\omega}_k$ as the integration is performed along the contours $\tilde{C}_k$ and $\tilde{C}_k^*$. The contribution

$$s_r(\mathbf{E}(\omega_0), \mathbf{E}^\circ(\omega_0)) = \frac{1}{2\pi i} \oint_{C_r} \frac{s(\mathbf{E}(\omega), \mathbf{E}^\circ(\omega))}{\omega - \omega_0} d\omega$$

is the remainder of the expansion containing nonresonant components as well as components corresponding to eigenfrequencies outside of the contour C_r.

The RPE is based on evaluating $s(\mathbf{E}(\omega), \mathbf{E}^\circ(\omega))$ by solving Eq. (1) for the frequencies ω and $-\omega$. Consequently, the quadratic form $s(\mathbf{E}(\omega), \mathbf{E}^\circ(\omega))$, where a product of $\mathbf{E}(\omega)$ and $\mathbf{E}^\circ(\omega)$ is involved, does not diverge. This is due to the cancellation of the factors $e^{i(n\omega/c)r}$ and $e^{-i(n\omega/c)r}$ of the fields in the far-field region, where $r = \|\mathbf{r}\|$. In this way, it becomes possible to compute modal expansions of far-field quantities with nondiverging expansion terms. To illustrate this, we consider a one-dimensional resonator and compute electric fields, $\mathbf{E}(x, \omega)$ and $\mathbf{E}^\circ(x, \omega)$, fulfilling the corresponding Helmholtz equation. Figures 1(a) and 1(c) sketch the diverging field $\mathbf{E}(x, \tilde{\omega}_{k,\Delta})$ and the nondiverging field $\mathbf{E}^\circ(x, \tilde{\omega}_{k,\Delta})$ outside of the resonator, respectively. The frequency $\tilde{\omega}_{k,\Delta} = \tilde{\omega}_k + \Delta\tilde{\omega}_k$ represents an evaluation point on an integration contour $\tilde{C}_k$. Figure 1(d) shows the nondiverging product $\mathbf{E}(x, \tilde{\omega}_{k,\Delta}) \cdot \mathbf{E}^\circ(x, \tilde{\omega}_{k,\Delta})$, which relates to the energy flux density. The approach also applies to arbitrary three-dimensional problems, where, in the far-field region, $\mathbf{E}(\mathbf{r}, \omega) \sim e^{i(n\omega/c)r}(1/r)$ and $\mathbf{E}^\circ(\mathbf{r}, \omega) \sim e^{-i(n\omega/c)r}(1/r)$.

III. APPLICATION

The presented approach is used for modal analysis of a quantum technology device. We revisit an example from the literature [38], where a quantum dot acts as a single-photon source. For a specific far-field region, the photon collection efficiency (PCE) has been enhanced by using a numerically optimized circular Bragg grating nanoresonator. Such devices can be realized experimentally by using deterministic fabrication technologies [39]. For more details on the specific device and material properties, the reader is referred to [38]. The geometry is sketched in Fig. 2(a). To numerically analyze the
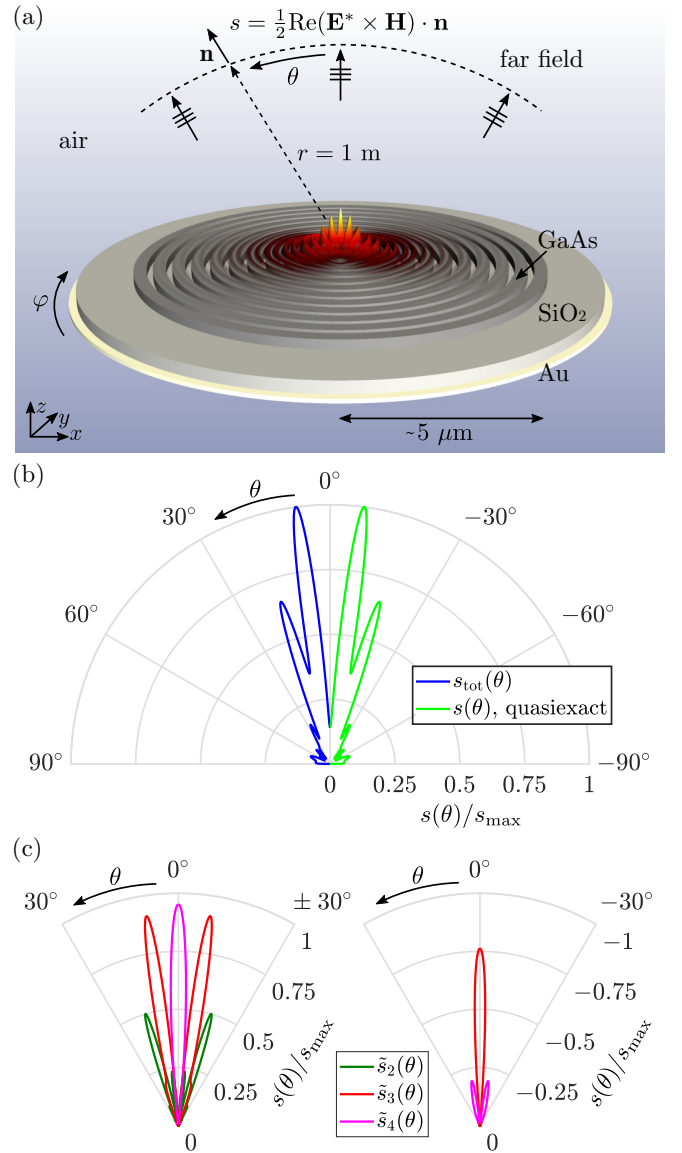

FIG. 2. Circular Bragg grating resonator with localized light source. (a) Geometry with an illustration of the electric field intensity (a.u.) of the QNM corresponding to the eigenfrequency $\tilde{\omega}_2$; see Table I. The gallium arsenide (GaAs) grating has a thickness of 240 nm and consists of an inner disk with a radius of 550 nm and 10 rings with a width of 340 nm and a periodicity of 500 nm. The grating is placed on a silicon dioxide (SiO$_2$) layer with a thickness of 240 nm, which is coated from below with a gold (Au) layer of 300 nm thickness. The light source is modeled by a dipole emitter placed at the center of the inner disk. The dipole radiates at the frequency ω_0 and is oriented in x direction. (b) Radiation diagram at $\omega_0 = 2\pi c/(1360$ nm$)$ for the total modal expansion $s_{\text{tot}}(\theta)$ computed by Eq. (2) and for the quasiexact solution of the energy flux density $s(\theta)$. The quantities are evaluated at $r = 1$ m and $\varphi = 90°$, which corresponds to the yz plane. (c) Modal decomposition of the radiation diagram for the contributions $\tilde{s}_2(\theta)$, $\tilde{s}_3(\theta)$, and $\tilde{s}_4(\theta)$.

light source, we spatially discretize the system with the finite element method (FEM) using the solver JCMSUITE [40].

The quantity of interest is the energy flux density in the far field $s(\omega_0, \theta) = s(\mathbf{E}(\omega_0, \theta), \mathbf{E}^\circ(\omega_0, \theta))$, see Eq. (2), where

θ is the inclination angle as shown in Fig. 2(a). For the modal expansion of $s(\omega_0, \theta)$, the outer contour C_r is chosen to enclose the wavelength range of interest, 1280 nm $\leqslant$ $\lambda_0 \leqslant 1400$ nm, where $\lambda_0 = 2\pi c/\omega_0$. We compute all eigenfrequencies inside of the contour, which are listed in Table I. Note that only those rotationally symmetric QNMs which can couple to the dipole source are computed. Figure 2(a) sketches the electric field intensity of the QNM corresponding to $\tilde{\omega}_2$ in the near field of the structure. The QNM exhibits a maximum of the field intensity at the center of the resonator and it diverges in the far-field region.

For a fixed dipole frequency, the radiation diagrams for the total modal expansion $s_{\text{tot}}(\omega_0, \theta) = \sum_{k=1}^{9} \tilde{s}_k(\omega_0, \theta) + s_r(\omega_0, \theta)$ and for the quasiexact solution $s(\omega_0, \theta)$ are depicted in Fig. 2(b). The quasiexact solution is computed by solving scattering problems given by Eq. (1) directly. The total modal expansion coincides with the quasiexact solution with an absolute error of $s(\theta)/s_{\text{max}} < 5 \times 10^{-3}$ and, for the angle region $-60° < \theta < 60°$, with a relative error smaller than 3×10^{-5}. The differences in these solutions are related to numerical discretization errors and would decrease further by refining the numerical parameters. The agreement demonstrates that, although the associated QNMs diverge in the far field, the RPE of the energy flux density gives correct results with nondiverging expansion terms. Figure 2(c) shows the modal energy flux densities $\tilde{s}_2(\omega_0, \theta)$, $\tilde{s}_3(\omega_0, \theta)$, and $\tilde{s}_4(\omega_0, \theta)$. These are the significant contributions for the total energy flux density and they have different directivities corresponding to the different diffraction intensities of the Bragg grating. The contributions $\tilde{s}_3(\omega_0, \theta)$ and $\tilde{s}_4(\omega_0, \theta)$ also have negative values. A negative modal energy flux density can be understood as suppression of light emission into specific directions arising from the interference of various modes excited by the source at the frequency ω_0. Negative modal contributions have been reported also for QNM expansions of near-field quantities [19]. Note that, as physically expected, the total modal expansion of the energy flux density, $s_{\text{tot}}(\omega_0, \theta)$, is positive for all angles θ.

Next, the RPE is used to obtain insight into the properties of the device for the wavelength range 1280 nm $\leqslant \lambda_0 \leqslant$ 1400 nm. Figure 3(a) shows the normalized decay rate, also termed Purcell enhancement,

$$\Gamma(\omega_0) = -\frac{1}{2}\text{Re}(\mathbf{E}(\omega_0) \cdot \mathbf{j}^*)/\Gamma_b,$$

where $\mathbf{j} = -i\omega\mathbf{p}$ with the dipole moment $\mathbf{p}$ and Γ_b is the dipole emission in homogeneous background material [17]. It can be observed that, in the wavelength range of interest, the three resonances corresponding to the eigenfrequencies $\tilde{\omega}_2$, $\tilde{\omega}_3$, and $\tilde{\omega}_4$ are significant for the Purcell enhancement. The resonance with the eigenfrequency $\tilde{\omega}_1$ has a very small influence. The nonresonant contributions and the contributions associated with other eigenfrequencies are negligible. Figure 3(b) shows the PCE,

$$\eta(\omega_0) = \frac{1}{P_{\text{DE}}} \int_{\delta\Omega} \frac{1}{2}\text{Re}\left(\mathbf{E}^*(\omega_0) \times \frac{1}{i\omega_0\mu_0}\nabla \times \mathbf{E}(\omega_0)\right) \cdot d\mathbf{S},$$

where $\delta\Omega$ is the far-field region corresponding to NA = 0.8 and P_{DE} is the emitted power of the dipole emitter into the upper hemisphere. In the case of the PCE, the resonances corresponding to $\tilde{\omega}_1$, $\tilde{\omega}_2$, $\tilde{\omega}_3$, and $\tilde{\omega}_4$ play an important role. In
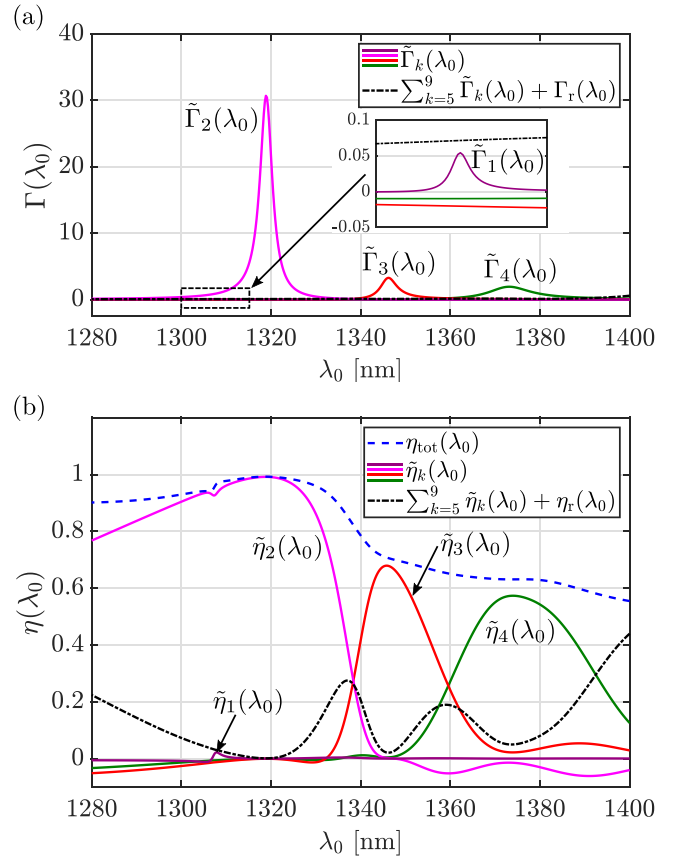

FIG. 3. Modal expansions of Purcell enhancement and PCE for the resonator with a localized light source shown in Fig. 2(a). Eigenfrequencies $\tilde{\omega}_1, \ldots, \tilde{\omega}_9$ are considered; see Table I. (a) Modal expansion of the Purcell enhancement. The contributions $\tilde{\Gamma}_1(\lambda_0), \ldots, \tilde{\Gamma}_4(\lambda_0)$ correspond to the eigenfrequencies $\tilde{\omega}_1, \ldots, \tilde{\omega}_4$, respectively. The remaining modal contributions are added to the remainder of the expansion $\sum_{k=5}^{9} \tilde{\Gamma}_k(\lambda_0) + \Gamma_r(\lambda_0)$. The term $\Gamma_r(\lambda_0)$ includes also modal contributions corresponding to eigenfrequencies outside the integration contour C_r. (b) Modal expansion of the PCE. Total modal expansion, $\eta_{\text{tot}}(\lambda_0) = \sum_{k=1}^{9} \tilde{\eta}_k(\lambda_0) + \eta_r(\lambda_0)$, single modal contributions, $\tilde{\eta}_1(\lambda_0), \ldots, \tilde{\eta}_4(\lambda_0)$, and the sum of other contributions, $\sum_{k=5}^{9} \tilde{\eta}_k(\lambda_0) + \eta_r(\lambda_0)$.

contrast to the Purcell enhancement, the modal contribution $\tilde{\eta}_1(\omega_0)$ is significant for the PCE. It contributes to $\eta_{\text{tot}}(\omega_0)$ for the wavelength region near to its maximum. Note that the behavior of the remaining contributions, $\sum_{k=5}^{9} \tilde{\eta}_k(\lambda_0) + \eta_r(\lambda_0)$, is partially based on resonances with eigenfrequencies outside the integration contour C_r.

IV. CONCLUSIONS

A theoretical approach to investigate modal quantities in the far field of resonant systems was presented. Although the QNMs decay exponentially in time and thus represent diverging outgoing waves, modal expansions can be computed rigorously. The approach was applied to expand the energy flux density in the far field of a nanoresonator with an embedded point source. It was demonstrated that, by computing modal far-field patterns, those resonances which contribute significantly to the scattering response of the nanophotonic

device can be identified. Thus deeper physical insights into the system are gained.

The method cannot only be used to efficiently compute the scattering response and to compare to experimental results, but also for an optimization of devices for a tailored functionality. It can be applied to far-field as well as to near-field quantities. Examples are quantities involving the electromagnetic energy flux density or the electromagnetic absorption. However, the investigations in this work are limited to quadratic forms with a sesquilinear map. We expect that, with resolving the key issue of the far-field treatment in QNM modeling, the presented approach will enable usage of QNMs in various fields. Applications include systems in nano-optics with any material dispersion and any resonant system in general, e.g., in acoustics or quantum mechanics.

[1] L. Novotny and N. van Hulst, Nat. Photon. **5**, 83 (2011).

[2] X. Ding, Y. He, Z.-C. Duan, N. Gregersen, M.-C. Chen, S. Unsleber, S. A. Maier, C. Schneider, M. Kamp, S. Höfling, C.-Y. Lu, and J.-W. Pan, Phys. Rev. Lett. **116**, 020401 (2016).

[3] Y. Zhang, S. He, W. Guo, Y. Hu, J. Huang, J. R. Mulcahy, and W. D. Wei, Chem. Rev. **118**, 2927 (2018).

[4] J. N. Anker, W. P. Hall, O. Lyandres, N. C. Shah, J. Zhao, and R. P. Van Duyne, Nat. Mater. **7**, 442 (2008).

[5] N. Yu and F. Capasso, Nat. Mater. **13**, 139 (2014).

[6] M. S. Tame, K. R. McEnery, S. K. Özdemir, J. Lee, S. A. Maier, and M. S. Kim, Nat. Phys. **9**, 329 (2013).

[7] A. I. Kuznetsov, A. E. Miroshnichenko, M. L. Brongersma, Y. S. Kivshar, and B. Luk'yanchuk, Science **354**, aag2472 (2016).

[8] C. W. Hsu, B. Zhen, A. D. Stone, J. D. Joannopoulos, and M. Soljačić, Nat. Rev. Mater. **1**, 16048 (2016).

[9] P. Lalanne, W. Yan, K. Vynck, C. Sauvan, and J.-P. Hugonin, Laser Photon. Rev. **12**, 1700113 (2018).

[10] P. T. Kristensen, K. Hermann, F. Intravaia, and K. Busch, Adv. Opt. Photon. (2020), doi:10.1364/AOP.377940.

[11] H. Lamb, Proc. London Math. Soc. **s1-32**, 208 (1900).

[12] G. Beck and H. M. Nussenzveig, Nuovo Cimento (1955-1965) **16**, 416 (1960).

[13] E. S. C. Ching, P. T. Leung, A. Maassen van den Brink, W. M. Suen, S. S. Tong, and K. Young, Rev. Mod. Phys. **70**, 1545 (1998).

[14] E. A. Muljarov, W. Langbein, and R. Zimmermann, EPL **92**, 50010 (2010).

[15] B. Vial, F. Zolla, A. Nicolet, and M. Commandré, Phys. Rev. A **89**, 023829 (2014).

[16] F. Zolla, A. Nicolet, and G. Demésy, Opt. Lett. **43**, 5813 (2018).

[17] L. Zschiedrich, F. Binkowski, N. Nikolay, O. Benson, G. Kewes, and S. Burger, Phys. Rev. A **98**, 043806 (2018).

[18] W. Yan, R. Faggiani, and P. Lalanne, Phys. Rev. B **97**, 205422 (2018).

[19] C. Sauvan, J.-P. Hugonin, I. S. Maksymov, and P. Lalanne, Phys. Rev. Lett. **110**, 237401 (2013).

[20] X. Zambrana-Puyalto and N. Bonod, Phys. Rev. B **91**, 195422 (2015).

[21] E. A. Muljarov and W. Langbein, Phys. Rev. B **94**, 235438 (2016).

[22] R. Colom, R. McPhedran, B. Stout, and N. Bonod, Phys. Rev. B **98**, 085418 (2018).

[23] M. I. Abdelrahman and B. Gralak, OSA Continuum **1**, 340 (2018).

[24] M. K. Dezfouli and S. Hughes, Phys. Rev. B **97**, 115302 (2018).

[25] P. Y. Chen, D. J. Bergman, and Y. Sivan, Phys. Rev. Appl. **11**, 044018 (2019).

[26] D. J. Bergman, Phys. Rev. B **19**, 2359 (1979).

[27] H. E. Türeci, A. D. Stone, and B. Collier, Phys. Rev. A **74**, 043822 (2006).

[28] R.-C. Ge, P. T. Kristensen, J. F. Young, and S. Hughes, New J. Phys. **16**, 113048 (2014).

[29] S. Franke, S. Hughes, M. K. Dezfouli, P. T. Kristensen, K. Busch, A. Knorr, and M. Richter, Phys. Rev. Lett. **122**, 213901 (2019).

[30] J. Yang, J.-P. Hugonin, and P. Lalanne, ACS Photon. **3**, 395 (2016).

[31] J. Ren, S. Franke, A. Knorr, M. Richter, and S. Hughes, Phys. Rev. B **101**, 205402 (2020).

[32] P. T. Kristensen, R.-C. Ge, and S. Hughes, Phys. Rev. A **92**, 053810 (2015).

[33] E. A. Muljarov and W. Langbein, Phys. Rev. A **96**, 017801 (2017).

[34] P. T. Kristensen, R.-C. Ge, and S. Hughes, Phys. Rev. A **96**, 017802 (2017).

[35] B. Stout, R. Colom, N. Bonod, and R. McPhedran, arXiv:1903.07183.

[36] F. Binkowski, L. Zschiedrich, M. Hammerschmidt, and S. Burger, Phys. Rev. B **100**, 155406 (2019).

[37] J. D. Jackson, *Classical Electrodynamics*, 3rd ed. (Wiley, New York, 1998).

[38] L. Rickert, T. Kupko, S. Rodt, S. Reitzenstein, and T. Heindel, Opt. Express **27**, 36824 (2019).

[39] P. Senellart, G. Solomon, and A. White, Nat. Nanotechnol. **12**, 1026 (2017).

[40] J. Pomplun, S. Burger, L. Zschiedrich, and F. Schmidt, Phys. Status Solidi B **244**, 3419 (2007).